Proceedings of the ASME 2012 Conference on Smart Materials, Adaptive Structures and Intelligent Systems
SMASIS2012
September 19-21, 2012, Stone Mountain, Georgia, USA

SMASIS2012-8257

ANALYSIS OF SHAPE MEMORY POLYMER-ALLOY COMPOSITES: MODELING AND PARAMETRIC STUDIES

Jungkyu Park **Leon M. Headings** **Marcelo J. Dapino**
Department of Mechanical and Aerospace Engineering, The Ohio State University, Columbus, Ohio, USA

Jeffery W. Baur
Air Force Research Laboratory, Materials and Manufacturing Directorate, Wright-Patterson Air Force Base, Ohio, USA

Gyaneshwar P. Tandon
University of Dayton Research Institute, Dayton, Ohio, USA

ABSTRACT

Shape memory composites (SMCs) based on shape memory alloys (SMAs) and shape memory polymers (SMPs) are interesting due to their controllable temperature-dependent mechanical properties. The complementary characteristics of SMAs and SMPs can be used to create materials or systems with shape recovery created by the SMA and shape fixity provided by the SMP. In this research, three SMC operating regimes are identified and the behavior of SMC structures is analyzed by focusing on composite fixity and interfacial stresses. Analytical models show that certain SMPs can achieve sufficient shape fixing. COMSOL Multi-Physics simulations are in agreement with analytical expressions for shape fixity and interfacial stresses. Analytical models are developed for an end-coupled linear SMP-SMA two-way actuation system.

Keywords: shape memory composite, shape memory polymer, shape memory alloy, shape fixity, interfacial stress, COMSOL

INTRODUCTION

Shape memory polymers (SMPs) are polymeric smart materials that can undergo large deformation when heated above the glass transition temperature T_g, fix the deformed shape when cooled below T_g, and subsequently recover the original shape when reheated above T_g. At temperatures below T_g, an SMP is in a glassy state exhibiting a high modulus and sufficient rigidity to resist deformation [1]. This effect can be used to provide shape fixity for shape memory composites (SMCs) composed of SMPs and shape memory alloys (SMAs). Conversely, an SMP is in a rubbery state with a low modulus above T_g and becomes highly deformable, exhibiting a large decrease in its Young's modulus. SMPs have several advantages over SMAs: they have a much lower density, larger strain recoverability up to 400%, and a lower manufacturing cost [2]. Due to these characteristics, SMPs have been researched as promising materials for morphing aircraft skins [3]. However, SMPs return to their memory shape with lower recovery forces than SMAs due to their material properties. In addition, their fatigue strength is lower than that of SMAs [4]. In order to improve these mechanical properties, SMP composites incorporating SMAs have been investigated [5, 6].

SMAs are ductile in their low temperature martensitic state and are able to undergo significant shape deformation until they are heated [7]. At high temperatures, SMAs are in an austenitic state and become elastic with a high modulus. Thus, they try to return to their memorized shape with high recovery force. SMAs generate large recovery stresses in a composite medium which depend on composition and pre-strain [8]. Under an applied stress, SMAs can exhibit superelastic behavior, which is a result of the transformation to stress-induced martensite. Characteristic SMA temperatures are austenite start and finish temperatures and martensite start and finish temperatures. Understanding the characteristics of SMAs and SMPs allows their complementary use in SMCs by exploiting the characteristic shape recovery of SMAs and the shape fixity of SMPs.

Tobushi et al. [5] fabricated an SMC belt using a polyurethane SMP sheet with an embedded TiNi SMA wire and

conducted three-point bending tests. In addition, Tobushi et al. made an SMC belt with a polyurethane SMP sheet and two TiNi SMP tapes to demonstrate two-way bending deformation [6]. Deformation tests at various temperatures show shape fixity with high rigidity at low temperature and shape recovery with large recovery force at high temperature.

In SMP-SMA composite applications, the geometries must be designed to provide the desired shape fixity and recovery while operating within appropriate stress and strain ranges for the specific materials used. The aim of this paper is to identify the SMC operating regimes and analyze the shape fixity and interfacial stresses for SMCs using analytical models and COMSOL finite element simulations. Three specific SMC geometries are examined, including an SMP matrix with an embedded SMA wire, SMP-SMA multi-layer bending structures, and end-coupled SMP-SMA linear systems. Parametric studies show the effects of SMC geometric parameters on shape fixity.

SMC OPERATING REGIMES

Three operating regimes of SMCs can be identified based on the relative transition temperatures of the SMP and SMA, that capitalize on the characteristic shape fixity of SMPs and shape recovery of SMAs: 1st) hold applied strains in the austenitic state or superelastic regime of the SMA, 2nd) lock positions in a multi-way SMA actuator, and 3rd) add stiffness to the otherwise ductile martensitic state of the SMA. The relative phase transition temperatures of the SMA and SMP for the three operating regimes are shown in Figure 1.

In the shape fixing cycle for the 1st operating regime, the SMP glass transition temperature range is higher than the SMA austenitic finish temperature A_f. The SMP is used to fix the position of an austenitic SMA spring. In this cycle, the SMC is: 1) heated above T_g (SMP in rubbery state), 2) deformed by an initial load, and 3) cooled below T_g ($M_s<T<T_g$, SMP in glassy state) to its fixed state. Shape fixity of the composite and internal stresses are analyzed in the final fixed state when the initial load is removed.

For locking positions in a multi-way SMA actuator, the 2nd SMC operating regime uses an SMP with a glass transition temperature range that ideally falls between the SMA martensite start (M_s) and austenite start (A_s) temperatures. Starting with the memorized lower temperature shape, the SMC may be: 1) heated above T_g but below A_s (SMA remains martensitic); 2) deformed by a preload spring or other load; and 3) cooled below T_g to fix the deformed shape. Next, the SMC may be: 4) heated above T_g to soften the SMP, then continue to be heated above A_f to recover the initial shape of the SMA; and 5) cooled below T_g to fix the recovered shape, and further cooled to below M_f. The SMP fixes the recovered shape before the SMA transitions to martensite. In this way, the SMP can be used to fix the two-way actuator at low temperatures in either the memorized or deformed shapes.

For low temperature stiffening of an SMA in the 3rd operating regime, the SMP glass transition temperature range is lower than the SMA martensite finish temperature M_f. In this regime, the SMP is used to add stiffness to the otherwise soft martensitic SMA. The SMA may be used in typical cycles and applications, but when cooled below T_g, the SMP adds stiffness to the current shape of the SMA. For example, if a counteracting spring were used with an SMA for two-way actuation, the SMA memory shape would be released before the SMP became rigid. However, the SMP would add rigidity to the deformed position, making it less sensitive to disturbances. While this regime is not examined in this paper, modeling could be done similar to the 1st regime, with the austenitic SMA spring force replaced by a ductile stress-strain model for a martensitic SMA.

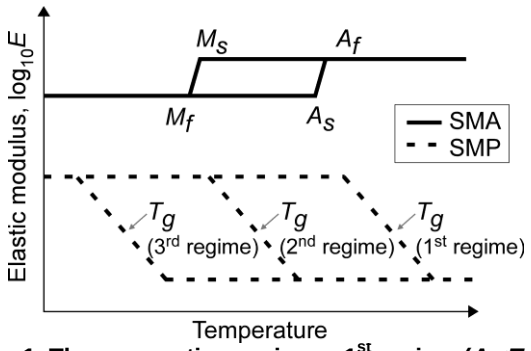

Figure 1. Three operating regimes: 1st regime ($A_f<T_g$), 2nd regime ($M_s<T_g<A_s$), and 3rd regime ($T_g<M_f$).

CASE I: SMP MATRIX WITH AN EMBEDDED SMA WIRE

The first geometry considered is an SMA wire spring embedded in an SMP bar with rectangular cross section. In the memorized state, the SMA wire is straight. The axial stresses in the SMA wire and interfacial shear stresses are examined analytically and using a finite element model for a compressive stress applied to the SMA wire. The compressive stress simulates the compression that the SMA wire would experience when undergoing shape recovery, though the analysis does not consider the thermomechanical process involved in the shape memory transformation.

Axial Stresses in SMA Wire and Interfacial Shear Stress

The axial stresses in the SMA wire and interfacial shear stresses were examined analytically and using a finite element model for a compressive stress applied to the SMA wire. For the finite element simulation using COMSOL, a 2.4mm prescribed displacement input was applied to both ends of the SMA wire, corresponding to 8% strain of the wire under free-free conditions. The strains of the SMA wire and SMP matrix were calculated in COMSOL and resulted in the deformed shape shown in Figure 2.

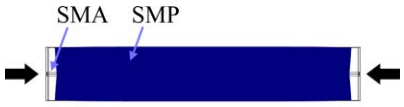

Figure 2. Deformation in *x-y* view (COMSOL).

Next, the shear lag model, which is widely used to analyze linear elastic stresses in short fiber composites [9], was employed in order to derive analytical expressions for axial stress and interfacial shear stress for the SMC. In the shear lag model, an external stress σ_0 is applied to both ends of the SMA wire only. In order to investigate the axial stress in the SMA and interfacial shear stress at a maximum compressive strain of 8%, the SMP is considered in its rubbery state ($T>T_g$).

The shear lag model assumes a cylindrical shape for the SMA wire and SMP matrix. Since the SMP matrix considered here is rectangular, two different cylinders with radii equal to the half-thickness (R_t=t/2) and half-width (R_w=w/2) of the rectangular matrix are considered instead. The shear lag model is used to calculate the axial stresses for each of the SMP radii. The average of the axial stresses for the two cases is then used to represent the axial stress of the original rectangular shape.

Figure 3a shows the unloaded SMC with straight dotted lines. The dotted lines on Figure 3b show the deformation caused by the axial stress σ_0. At the outer SMP radius R, the displacement of the SMP matrix is u_R, and at the outer SMA radius r, the displacement of the interface is u_r. The deformation u_R varies along the length because the surface boundary condition of the SMP matrix is free.

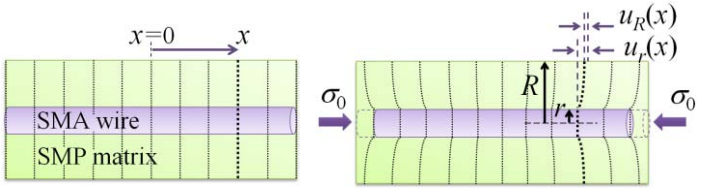

(a) (b)

Figure 3. (a) Unloaded SMC and (b) deformation in *x*-*z* view (shear lag model).

Figure 4 shows the free body diagram of a wire element and the shear strain in the matrix.

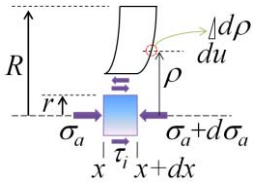

Figure 4. Free body diagram of a wire element and shear strain in the matrix.

The shear stress at the interface can be found from the force balance on the wire element shown in Figure 4,

$$2\pi r(dx)\tau_i = -\pi r^2(d\sigma_a) \quad \rightarrow \quad \frac{d\sigma_a}{dx} = -\frac{2\tau_i}{r} \tag{1}$$

If an annulus in the SMP matrix is considered with an inner radius r_1, outer radius r_2, and length dx, the shear forces acting at the two radii are equal [9],

$$2\pi r_1\tau_1 dx = 2\pi r_2\tau_2 dx \quad \rightarrow \quad \frac{\tau_1}{\tau_2} = \frac{r_2}{r_1} \tag{2}$$

From this relationship, the shear stress τ in the matrix at any radius ρ can be related to the interfacial shear stress τ_i at radius r. Therefore, $\tau = \tau_i(r/\rho)$. The shear strain γ in the matrix is expressed as $du/d\rho$ where u is the displacement of the matrix in the x direction. The shear strain is written in terms of the shear stress τ and the shear modulus G_p. The subscripts p and a denote the SMP matrix and the SMA wire, respectively.

$$\frac{du}{d\rho} = \gamma = \frac{\tau}{G_p} = \frac{\tau_i}{G_p}\left(\frac{r}{\rho}\right) \tag{3}$$

The shear modulus G_P is $0.5E_P/(1+\nu_P)$, where E_p is the elastic modulus and ν_p is the Poisson's ratio of the SMP. By integrating (3), the difference between the displacement u_R and u_r can be found.

$$\int_{u_r}^{u_R} du = \frac{\tau_i r}{G_p}\int_r^R \frac{d\rho}{\rho} \quad \rightarrow \quad u_R - u_r = \frac{\tau_i r}{G_p}\ln\left(\frac{R}{r}\right) \tag{4}$$

Solving (4) for τ_i and substitution into (1), the differential of σ_a with respect to x can be written

$$\frac{d\sigma_a}{dx} = -\frac{2(u_R - u_r)}{r^2\ln(R/r)}G_p = \frac{n^2}{r^2}(u_r - u_R)E_a \tag{5}$$

where $n = \left[E_p \Big/ \left(E_a(1+\nu_p)\ln(R/r)\right)\right]^{\frac{1}{2}}$.

Differentiating (5) and substitution of the boundary conditions leads to

$$\frac{d^2\sigma_a}{dx^2} = \frac{n^2}{r^2}(\varepsilon_a - \varepsilon_p)E_a = \frac{n^2}{r^2}(\sigma_a - \varepsilon_p E_a) \tag{6}$$

where the boundary conditions are $du_r/dx = \varepsilon_a = \sigma_a/E_a$ and $du_R/dx = \varepsilon_p$.

The top surface of the SMP matrix deforms and the strain ε_p varies along the SMA wire. The analytical solution of the second-order linear differential equation (6) is written as

$$\sigma_a = \varepsilon_p E_a + C_1\exp\left(\frac{n}{r}x\right) + C_2\exp\left(-\frac{n}{r}x\right) \tag{7}$$

The constants C_1 and C_2 are obtained by applying the boundary conditions $\sigma_a = -\sigma_0$ at $x = \pm L/2$. The constants C_1 and C_2 are equal.

$$C_1 = C_2 = -(\sigma_0 + \varepsilon_p E_a)\frac{\exp\left(-\frac{nL}{2r}\right) - \exp\left(\frac{nL}{2r}\right)}{\exp\left(-\frac{nL}{r}\right) - \exp\left(\frac{nL}{r}\right)} \tag{8}$$

Equation (1) shows the relationship between interfacial shear stress and axial stress. The interfacial shear stress τ_i along the SMA wire length can be found from (1) after differentiating (7) with respect to x. The shear stress is given by

$$\tau_i = -\frac{r}{2}\frac{d\sigma_a}{dx} = -\frac{r}{2}\left[\frac{C_1 n}{r}\exp\left(\frac{n}{r}x\right) - \frac{C_2 n}{r}\exp\left(-\frac{n}{r}x\right)\right] \tag{9}$$

The specific geometry examined was a straight SMA wire with radius r=0.375mm embedded in the center of a rectangular SMP matrix with dimensions L=60mm, t=4.2mm and w=10mm. First, the radius R is considered to be equal to the beam half–thickness R_t. The COMSOL model uses a prescribed displacement of 2.4mm at the ends of the SMA wire to achieve an 8% strain. This strain corresponds to an applied stress of σ_0 =5.67GPa which was used for the shear lag model. The first boundary condition du_r/dx is constant along the length of the SMA wire.

$$\frac{du_r}{dx} = \varepsilon_a = \frac{2.4\text{mm}}{30\text{mm}} = 8\% \tag{10}$$

The second boundary condition du_R/dx varies along the SMA wire. Data points are chosen to match the axial stresses from COMSOL simulations. The data points and curve fit are plotted in Figure 5a.

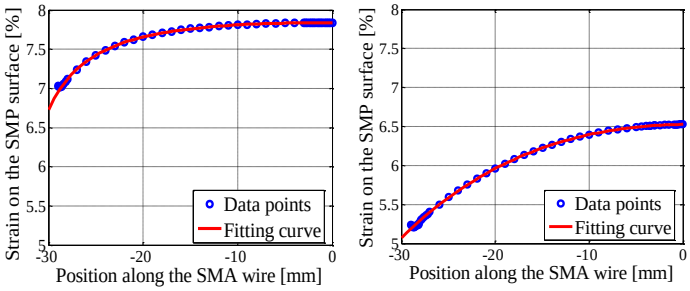

Figure 5. Strain on the SMP surface: (a) $R=R_t$ and (b) $R=R_w$.

The curve fit equation is

$$\frac{du_R}{dx} = \varepsilon_p = \frac{p_1 x^2 + p_2 x + p_3}{x + q_1} \qquad 0 \le x \le 30\,\text{mm} \tag{11}$$

The stress input σ_0 and boundary condition (11) are used to calculate the constants C_1 and C_2 from (8). These constants are used for the analytical calculations of axial stress (7) and interfacial shear stress (9).

Next, the radius R is considered to be equal to the half-width R_w. As with the previous calculation, du_r/dx is 8% but now corresponds to an applied stress input of 5.91 GPa. Also, du_R/dx varies along the SMA wire and data points are chosen to match the axial stresses obtained from the COMSOL simulation. The data points and curve fit are plotted in Figure 5b.

Finally, the axial stresses calculated using the shear lag model for radii of R_t and R_w are averaged in order to approximate the axial stress of the rectangular-shaped SMP. Figure 6 shows the COMSOL simulation results and the predicted shear lag model results for the rectangular-shaped SMP matrix. The shear lag model results match well with the COMSOL results. Due to stress concentrations at the ends of the structure, the COMSOL stress data for the first 1mm from both ends are not considered and not shown in figures. The shear lag model neglects the stress concentration at the ends [10] and therefore produces a smooth stress curve near the ends of the SMA wire.

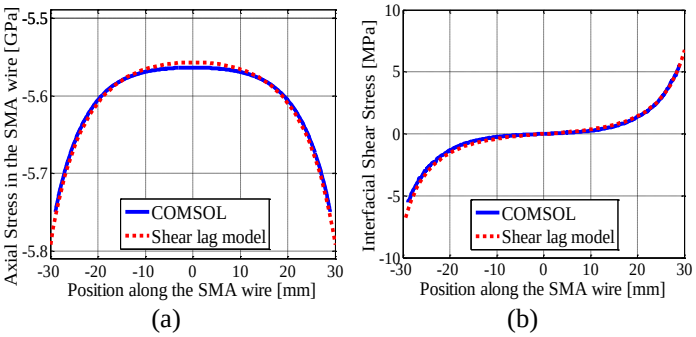

Figure 6. (a) Axial stress in the SMA wire and (b) shear stress at the interface for a rectangular-shaped SMP matrix.

CASE II: SMP-SMA-SMP MULTI-LAYER CANTILEVER BEAM (1ST REGIME OF SMC)

An SMP-SMA-SMP multi-layer cantilever beam is examined as the second geometry, operating in the 1st SMC regime. Analytical expressions for shape fixity and interfacial shear stress are confirmed by COMSOL finite element simulations.

Deflection and Shape Fixity of SMP-SMA-SMP Multi-layer Composite Beam ($T>A_f$)

This section consists of two parts: 1) development of an analytical model for deflection and shape fixity of an SMP-SMA-SMP multi-layer composite beam, and 2) comparison of analytical model results with COMSOL simulation results. In order to deform the composite layers, the beam is loaded with a downward force P at the end of the SMA layer (Figure 7), which is in its austenitic state ($T>A_f$). The opposite end of the composite beam is fixed.

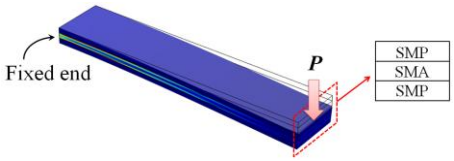

Figure 7. Deflection of the SMP-SMA-SMP multi-layer composite beam.

Analytical Model for Deflection and Shape Fixity of an SMP-SMA-SMP Multi-layer Composite Beam

The beam bending models used here assume linear elastic deformation, incompressible materials, small deflections, and that shape fixity of the SMP by itself is neglected. The initial point loading of the structure leads to a uniformly distributed restoring force in the SMA layer. This restoring force is considered as applied to the SMP in its glassy state in order to determine the amount of deformation from the loaded shape to the fixed shape when unloaded. While the distributed restoring force acts to straighten the bent structure, due to the assumption of small deflections, the deformation can be calculated as a distributed load applied to a straight beam.

First, the deformation of the beam is calculated for a load P applied at the tip of the beam, as shown in Figure 8a. For this model, it is assumed that the stiffness of the SMP is negligible when $T>T_g$, so only the SMA layer of the beam needs to be considered for the initial deformation.

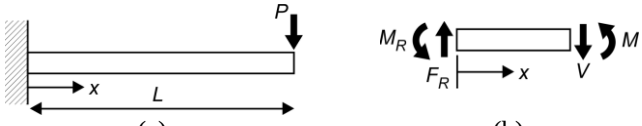

Figure 8. (a) Cantilever beam loaded with force P and (b) free-body diagram of the beam segment.

The moment in the beam with length L is

$$M(x) = -M_R + F_R x = -PL + Px \tag{12}$$

where $M_R=PL$ and $F_R=P$ are the reaction moment and reaction force, respectively. For beam bending, the internal bending moment $M(x)$ can be written as

$$M(x) = E_{A2} I_A \frac{d^2 v}{dx^2} \tag{13}$$

where E_{A2} is the Young's modulus of the SMA at $T>A_f$ and I_A is the area moment of inertia of the SMA layer cross-section. By substituting (12) into (13) and integrating twice with respect to x, the deflection $v(x)$ from the SMA layer only is obtained as

$$v(x) = \frac{P}{6E_{A2}I_A}\left(x^3 - 3Lx^2\right) \tag{14}$$

using the boundary conditions $dv/dx=0$ and $v=0$ at $x=0$. While the deflection equation (14) relates the deflection to the applied force P, the resulting shear forces F_A within the SMA can be thought of as restoring shear forces which vary as a function of deflection. So, from (14), the distributed shear force in the SMA that acts on the SMP and varies with deflection can be written as

$$F_A = \frac{6E_{A2}I_A v(x)}{x^3 - 3Lx^2} \tag{15}$$

The SMP layer is considered as "added" when cooled to $T<T_g$ (still $T>M_s$).

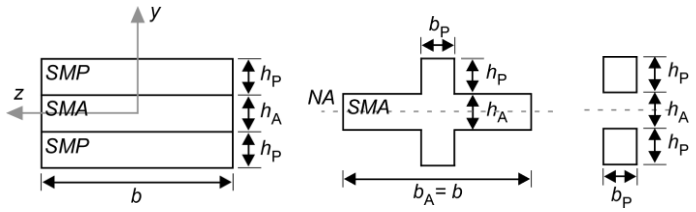

Figure 9. (a) Cross section of SMP-SMA composite, (b) equivalent structure with a single material, and (c) transformed SMP-equivalent sections.

Standard beam bending equations can be used for composite beams by converting the beam to an equivalent geometry for a single material [11]. Here, the two SMP layers are transformed into equivalent layers of SMA (Figure 9a-b). Since the elastic modulus of SMPs is much lower than that of SMAs, the widths of the SMP layers are reduced for the equivalent geometry. The equivalent width is $b_P=nb_A$, where n is a transformation factor which has a value of E_{P1}/E_{A2}. E_{P1} is the Young's modulus of the SMP at $T<T_g$.

The neutral axis is at $y=0$ due to symmetry and the area moment of inertia about $y=0$ for the total SMP-equivalent beam (Figure 9b) is

$$I_e = \frac{b_A h_A^3}{12} + \frac{b_P h_P^3}{6} + \frac{b_P h_P}{2}\left(h_A + h_P\right)^2 \tag{16}$$

where h_A is the thickness of the SMA layer and h_P is the thickness of each SMP layer.

Because the SMA is treated as a shear stress applied to the SMP portion of the structure, only the SMP-equivalent sections are considered for the bending reaction (Figure 9c). The area moment of inertia about $y=0$ for only the SMP-equivalent beam (Figure 9c) is

$$I_{Pe} = \frac{b_P h_P^3}{6} + \frac{b_P h_P}{2}\left(h_A + h_P\right)^2 \tag{17}$$

The uniform shear force F_P is considered and the moment $M=F_P(L-x)$ is applied to the SMP-equivalent beam. While the deflection $v_2(x)$ is calculated for a straight SMP beam (Figure 10a), the deflection $v_2(x)$ is considered relative to the initial deformed shape $v_0(x)$, as shown in Figure 10b. This is reasonable due to the assumption of small deflections.

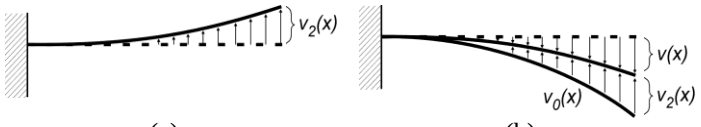

Figure 10. (a) Calculated deflection $v_2(x)$ of SMP-equivalent structure and (b) initial deflection $v_0(x)$ and final fixed deflection $v(x)$: $v_0(x) - v_2(x)$.

The internal bending moment for the SMP-equivalent structure is written in terms of the Young's modulus E_{A2} of the SMA material since the equivalent geometry is used to determine the area moment of inertia I_{Pe}.

$$M(x) = E_{A2} I_{Pe} \frac{d^2 v_2}{dx^2} = F_P x - F_P L \tag{18}$$

Integrating (18) twice with respect to x leads to

$$v_2(x) = \frac{F_P}{6E_{A2}I_{Pe}}\left(x^3 - 3Lx^2\right) \tag{19}$$

for the boundary conditions $dv_2/dx=0$ and $v_2(x)=0$ at $x=0$.

From (19), the restoring force F_P of the SMP can be determined for a given displacement. Since $v_2(x)=v_0(x)-v(x)$, F_P is written in terms of the original coordinates $v(x)$.

$$F_P = \frac{6E_{A2}I_{Pe}\left(v_0(x) - v(x)\right)}{x^3 - 3Lx^2} \tag{20}$$

Next, equating the "spring" forces F_A and F_P gives

$$\left[\frac{6E_{A2}I_A}{x^3 - 3Lx^2} + \frac{6E_{A2}I_{Pe}}{x^3 - 3Lx^2}\right] v(x) = \frac{6E_{A2}I_{Pe}}{x^3 - 3Lx^2} v_0(x) \tag{21}$$

So, the final fixed deflection $v(x)$ of the composite multi-layer beam relative to an initial deformation $v_0(x)$ is

$$v(x) = \left(\frac{I_{Pe}}{I_A + I_{Pe}}\right) v_0(x) \tag{22}$$

where $v_0(x) = \frac{P_0}{6E_{A2}I_A}\left(x^3 - 3Lx^2\right)$.

Since shape fixity is defined as the ratio of the final strain (after cooled to $T<T_g$ and the initial load removed) to the strain due to the initial applied load at $T>T_g$, the shape fixity for the composite is

$$RF_C = \frac{v(x)}{v_0(x)} = \frac{I_{Pe}}{I_A + I_{Pe}} \tag{23}$$

where RF_C indicates the ratio of the shape fixity for the SMC and I_{Pe} is the area moment of inertia of the SMP-equivalent geometry for the SMP. Substituting the equivalent geometry transformation equation $b_P=(E_{P1}/E_{A2})b_A$ into (17), the area moment of inertia I_{Pe} for the SMP-equivalent geometry can be written as

$$I_{Pe}=\frac{E_{P1}b}{6E_{A2}}\left(4h_P^3+6h_P^2h_A+3h_Ph_A^2\right) \tag{24}$$

The shape fixity of the multilayer composite beam can also be expressed in terms of a modulus ratio $R_E=E_{P1}/E_{A2}$ and a thickness ratio $R_h=h_P/h_A$.

$$RF_C=\frac{I_{Pe}}{I_A+I_{Pe}}=\frac{R_E\left[8R_h^3+12R_h^2+6R_h\right]}{1+R_E\left[8R_h^3+12R_h^2+6R_h\right]} \tag{25}$$

Comparison of Analytical Model Results with COMSOL Simulation Results

The parameter values used for the analytical model equations are E_{A2}=70GPa, E_{P1}=1.15GPa, b_A=10mm, b_P=10mm, h_A=1mm, h_P=1~10mm, L=50mm, and P=50N. The deflection of the composite beam is calculated from (22) and the shape fixity for the composite is obtained from (25).

While the analytical model uses a force input, the COMSOL simulation uses a downward stress input applied at the end surface area of the SMA layer. Since the cross-section of the SMA layer does not vary, the applied stress is constant along the length of the beam and calculated as $P/(b_Ah_A)$. The cross-sectional area of the SMA layer is 10^{-5}m^2, so the applied point loads P=5N, 25N, and 50N correspond to stress values of 0.5MPa, 2.5MPa, and 5MPa, respectively. The material property and geometry values used for the COMSOL simulation are the same as those used for the analytical model. In addition, the COMSOL simulation uses the Poisson's ratio and density. For the SMA and SMP materials, the Poisson's ratio is 0.3 and 0.35, and density is 6.45g/cm^3 and 1g/cm^3, respectively.

The final fixed deflection for an initial load P_0=5N is calculated analytically using (22) for thickness ratios ranging from 1 to 10 and plotted in Figure 11a. $R_h=h_P/h_A$ is the thickness ratio of the SMP to SMA layers. R_h=0 means that the thickness h_P of the SMP layer is zero and that only the SMA layer is considered. The deflection at R_h=0 corresponds to the initial deformed shape $v_0(x)$, but the final fixed deflection equals the initial shape before loading since there is no SMP to fix the shape. Using COMSOL, the final fixed deflection was calculated for the same conditions and plotted in Figure 11b. The analytical calculations and COMSOL simulations show good agreement.

Shape fixity at the tip was calculated by dividing the tip deflection of the fixed shape at each R_h by the initial tip deflection at R_h=0. The results for the COMSOL simulation and analytical model are plotted in Figure 12 and show good agreement. The errors in shape fixity between the analysis and COMSOL are less than 0.2%. When $R_h\geq6$, the shape fixity is greater than 97%. Shape fixity is load-independent but is a function of moment of inertia as shown in (23).

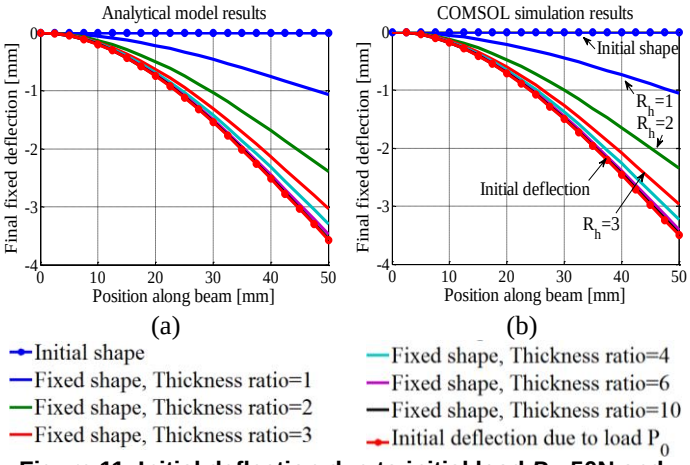

Figure 11. Initial deflection due to initial load P_0=50N and final fixed deflections for different thickness ratios: (a) analytical model and (b) COMSOL simulation.

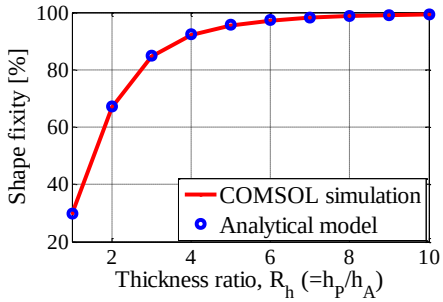

Figure 12. Shape fixity for various thickness ratios: COMSOL simulation results and analytical model results.

Interfacial Stress Analysis of SMP-SMA-SMP Multi-layer Composite Beam

Analytical models for normal stresses and shear stresses at the interface are derived by assuming small deflections. The analytical results are then compared with COMSOL simulation results.

Normal Stresses in the SMA Layer at the Interface

Normal stresses in the SMA layer at the interface are analyzed along the composite beam length as shown in Figure 13b (thick solid line). Point B is located in the SMA layer at the interface.

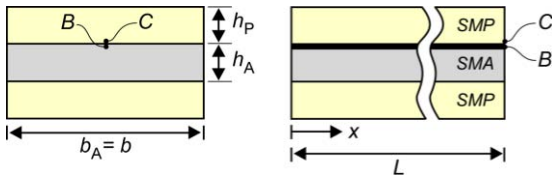

Figure 13. Points *B* and *C* at the SMP-SMA interface: (a) cross-section of beam and (b) beam length.

The axial normal stresses in the SMA layer at the interface are calculated from the following equation:

$$\sigma_B(x)=\frac{-M(x)y_B}{I_e}=\frac{\left(PL-Px\right)\left(h_A/2\right)}{\frac{b_Ah_A^3}{12}+\frac{b_Ph_P^3}{6}+\frac{b_Ph_P}{2}\left(h_A+h_P\right)^2} \tag{26}$$

where $y_B=h_A/2$. $M(x)$ and I_e are given by (12) and (16), respectively. The normal stresses $\sigma_B(x)$ are plotted and compared with COMSOL results in Figure 14a at a thickness ratio of R_h=6. When R_h=6, the shape fixity is greater than 97%.

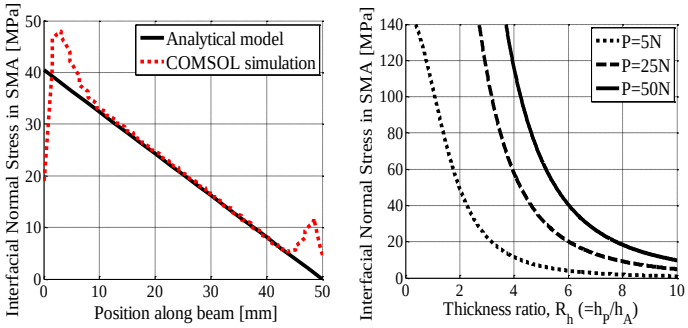

(a) (b)

Figure 14. (a) Normal stress in SMA: analytical model and COMSOL simulation at *P*=50N and R_h=6; (b) maximum normal stress vs. thickness ratio from analytical model.

The analytical model results in Figure 14a show that axial normal stresses decrease linearly along the beam length from the fixed end to the free end. Analytical model and COMSOL simulation results show good agreement for normal stresses except at both ends of the composite beam. This is due to stress concentrations at the ends which are not represented in the analytical model. Figure 14b shows the maximum interfacial normal stresses in the SMA layer, which occur at the fixed end, versus the thickness ratio. When R_h increases, the maximum normal stress in the SMA at the interface decreases. In order to satisfy the small deflection assumption, the slope of the deflection curve should be $dv/dx<0.1$. All points plotted in Figure 14b satisfy this criterion but, for example, a thickness ratio of 3 with a load of 50N does not.

The normal stress at point B in Figure 13 corresponds to a tensile stress. Normal stresses at the lower interface are compressive stresses, because the neutral axis is located in the middle of the composite beam. The analytical model results were compared with the tensile strength of Nitinol SMA. In the high temperature state, tensile yield strength of a Nitinol SMA is 560MPa and ultimate tensile strength is 754-960MPa [12]. Normal stresses in the SMA at the interface should be less than the yield strength in order to prevent irreversible damage. Thus, in addition to designing for shape fixity, the maximum normal stress in the SMA layer at the interface should be considered when designing the thickness of the SMP layers.

Shear Stresses in the SMP Layer at the Interface

Shear stresses in the SMP layer at the interface are analyzed along the length of the beam as shown in Figure 13b. Shear stresses in composite beams can be calculated using the shear formula (27) where $Q_{C'e}$ and I_e are calculated from the equivalent (all SMA) structure and b is the width of the original composite's cross section. C is a point in the SMP layer at the interface while C' indicates a point in the equivalent structure.

$$\tau_C(x)=\frac{V(x)Q_{C'e}}{I_e b}=\frac{P\left(h_A+h_P\right)b_P h_P}{2I_e b} \qquad (27)$$

where the shear force $V(x)$ is constant along the length for a point load P applied at the end of the beam. $Q_{C'e}=\bar{y}'A'$ where A' is the area of the equivalent structure that is above the stress measurement point and $\bar{y}'$ is the distance from the neutral axis to the center of A', as shown in Figure 15.

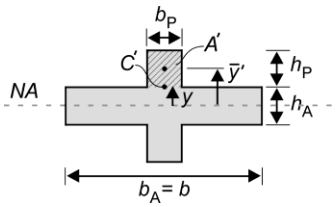

Figure 15. Equivalent SMA structure to the SMP-SMA-SMP composite.

While the analytical model (27) assumes constant shear stress across the width of the beam, the COMSOL simulation results in Figure 16 show that there is a considerable variation in shear stress across the beam. This is expected for beams that are wide relative to their thickness. The analytical model must therefore be interpreted as providing the average shear stress across the width of the beam rather than the maximum shear stress for each position along the beam.

From the COMSOL simulation results, the average shear stress was calculated for 1mm segments along the length of the beam and plotted with the analytical model results in Figure 17a. The analytical model (27) shows that shear stress at the interface is constant along the beam length. The COMSOL simulation also gives nearly constant shear stress results along the length of the composite beam except for the locations near both ends. As with the normal stresses in the previous section, this is due to stress concentrations in the COMSOL model which are not captured by the analytical model.

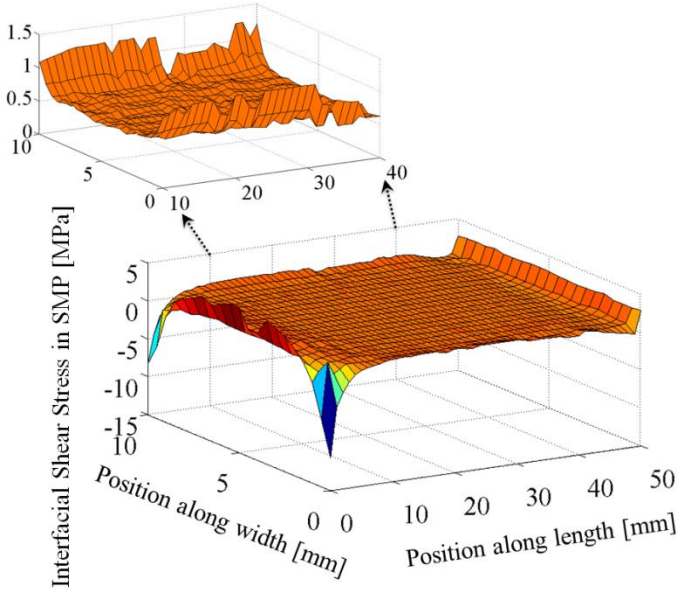

Figure 16. Interfacial shear stress: 3D plot using COMSOL simulation results.

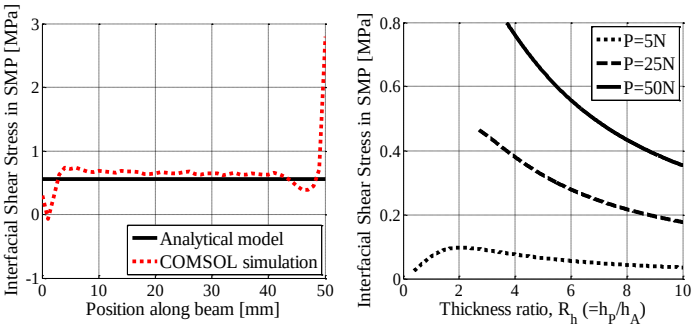

(a) (b)

Figure 17. (a) Shear stress in SMP: analytical model and COMSOL simulation at *P*=50N and R_h=6; (b) shear stress vs. thickness ratio from analytical model.

Shear stress values from the analytical model are plotted versus thickness ratio in Figure 17b for three different loads. Again, the points plotted all satisfy the criterion for the small deflection assumption. As seen in (27), shear stress is proportional to the applied force. The maximum shear stress for the plotted conditions is 0.8MPa when the load P is 50N and the thickness ratio R_h is 3.7. In this case, the tip deflection is 3.3mm. This maximum shear stress value is less than the ultimate shear strength of Veriflex SMP, which has been cited as 4.38MPa at room temperature (in a glassy state) [13].

Both shear strength in the SMP and normal strength in the SMA at the interface should be considered when designing the thickness ratio. At this maximum shear stress condition (P=50N and R_h=3.7), the normal stress in the SMA at the interface is approximately 140Ma (see Figure 14b). This value is less than the ultimate tensile stress (0.96GPa) of Nitinol SMA.

CASE III: END-COUPLED LINEAR SMP-SMA TWO-WAY ACTUATION SYSTEM (2ND REGIME OF SMC)

The third geometry considered is an end-coupled linear SMP-SMA system. First, the ability of the SMP to hold the deformed shape of the SMA is examined (1st regime of SMC operation). An analytical expression for the shape fixity of the composite structure is derived which includes the shape fixity of the SMP by itself. Next, the linear SMP-SMA system is considered with an additional spring as a two-way actuation system (2nd regime of SMC operation). This two-way actuation system is able to use the SMP to fix the actuator in two different positions at room temperature: *martensite fixed extended* and *martensite fixed compressed*.

Shape Fixity of Linear SMP-SMA System

First, the shape fixity of a linear SMP–SMA system is considered in the 1st regime of operation, with the SMA remaining austenitic throughout the cycle. The SMP and SMA are considered to be end-coupled and act in parallel as illustrated in Figure 18a.

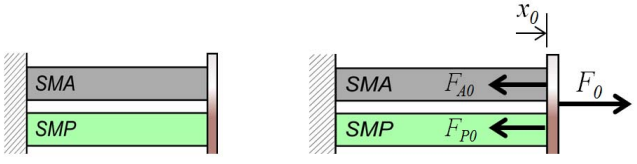

(a) (b)

Figure 18. Linear system fixity: (a) natural state and (b) step 0 ($T>T_g$).

In step 0 ($T>T_g$), an applied load F_0 causes an initial displacement x_0, shown in Figure 18b. A force balance gives

$$F_0 = F_{A0} + F_{P0} = k_{Aa}x_0 + k_{Ph}x_0 \quad \rightarrow \quad x_0 = \frac{F_0}{k_{Aa} + k_{Ph}} \tag{28}$$

where k_{Aa} is the stiffness of the SMA in its austenitic state, k_{Pl} is the stiffness of the SMP at low temperatures ($T<T_g$), and k_{Ph} is the stiffness of the SMP at high temperatures ($T>T_g$).

In step 1, the system is cooled below T_g ($M_s<T<T_g$) at constant strain. In step 2 ($T<T_g$), the fixed strain (at displacement x_0) is removed (Figure 19a).

(a) (b)

Figure 19. Linear system fixity: (a) step 2 ($T<T_g$) and (b) neutral position of SMP.

An SMP has an inherent shape fixity RF_P.

$$RF_P = \frac{\varepsilon_u}{\varepsilon_m} = \frac{x_u}{x_0} \tag{29}$$

where ε_u is the final strain after unloading and ε_m is the maximum strain. Thus, the SMP's new "neutral" position is $x_u = RF_P x_0$ (Figure 19b). With the applied force removed, the system reaches equilibrium when $F_{A2}=F_{P2}$.

$$F_{A2} = k_{Aa}x_2,\ F_{P2} = k_{Pl}(x_u - x_2) \rightarrow x_2 = \frac{k_{Pl}}{k_{Aa} + k_{Pl}} RF_P x_0 \tag{30}$$

By substituting x_0 from (29), the final fixed displacement can be expressed as

$$x_2 = RF_P \left(\frac{k_{Pl}}{k_{Aa} + k_{Pl}} \right) \left(\frac{F_0}{k_{Aa} + k_{Ph}} \right) \tag{31}$$

The shape fixity of the composite (with an SMP shape fixity of RF_P) is therefore

$$RF_C = \frac{x_2}{x_0} = RF_P \left(\frac{k_{Pl}}{k_{Aa} + k_{Pl}} \right) \tag{32}$$

Two-Way Actuation of Linear SMP-SMA System

Next, a linear end-coupled two-way actuation system is considered which includes an additional spring element. The system operates in the 2nd regime of operation, with the SMP glass transition temperature range falling between M_s and A_s. The natural states of the components are illustrated in Figure 20a. The natural lengths are defined at room temperature (RT) with the SMA in its martensitic state.

For the numerical modeling of this system, SMA stress-strain nonlinearities were modeled using stress saturation limits which are not reflected in the following equations. SMAs in both martensitic and austenitic states have a limited elastic stiffness range above which they strain at a relatively constant stress due to detwinning and stress-induced martensite transformations, respectively. In the numerical model, if an

applied strain exceeded the elastic range, the elastic force F_A was saturated at the appropriate constant maximum force. The model applied strain limits to ensure that the constant stress response region was not exceeded.

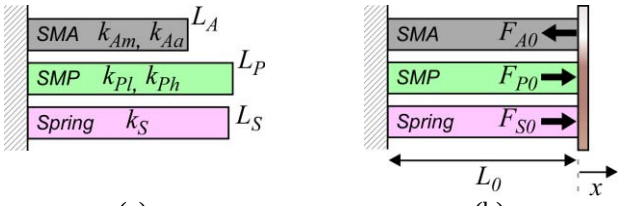

Figure 20. Two-way actuation: (a) natural states and (b) step 0.

In Step 0 (T_g<T<A_s), an end-cap is added, with the spring and the SMP in its rubbery state acting to stretch the martensitic SMA. The initial system length L_0 results from the force balance, as illustrated in Figure 20b.

$$F_{A0} = k_{Am}\left(L_0 - L_A\right), \quad F_{P0} = k_{Ph}\left(L_P - L_0\right)$$
$$F_{S0} = k_S\left(L_S - L_0\right), \quad L_0 = \frac{k_{Am}L_A + k_{Ph}L_P + k_S L_S}{k_{Am} + k_{Ph} + k_S} \tag{33}$$

In Step 1 (M_s<T<T_g), the system is cooled below T_g but remains above M_s, with the SMP helping to fix the position. The new force balance results in the position x_1 (Figure 21a). x_{Pn1} is the neutral position of the cooled SMP and RF_P indicates the shape fixity of the SMP.

$$F_{A1} = k_{Am}\left(L_0 - L_A + x_1\right), \quad F_{P1} = k_{Pl}\left(x_{Pn1} - x_1\right)$$
$$F_{S1} = k_S\left(L_S - L_0 - x_1\right), \quad x_{Pn1} = \left(L_P - L_0\right)\left(1 - RF_P\right)$$
$$x_1 = \frac{k_{Am}\left(L_A - L_0\right) + k_{Pl}x_{Pn1} + k_S\left(L_S - L_0\right)}{k_{Am} + k_{Pl} + k_S} \tag{34}$$

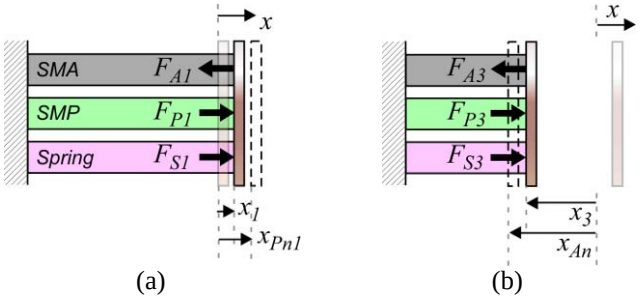

Figure 21. Two-way actuation: (a) step 1 and (b) step 3.

In Step 2 (T=RT<M_f), the system is cooled to room temperature, with a minimal change in position (x_2≈x_1) because the SMA was already martensitic. This step results in the first room temperature fixed position: *martensite fixed extended*.

In Step 3 (T>A_f), the system is heated through T_g then, with the SMP in its rubbery state, the SMA contracts as it continues to be heated from A_s to A_f and converts to its austenitic state (Figure 21b). The force balance is again used to calculate the resulting position x_3, where the internal force of the extended SMA is calculated relative to its neutral position x_{An}, based on its unloaded length L_A.

$$F_{A3} = k_{Aa}\left(x_3 - x_{An}\right), \quad F_{P3} = k_{Ph}\left(L_P - L_0 - x_3\right)$$
$$F_{S3} = k_S\left(L_S - L_0 - x_3\right), \quad x_{An} = L_A - L_0$$
$$x_3 = \frac{k_{Aa}x_{An} + k_{Ph}\left(L_P - L_0\right) + k_S\left(L_S - L_0\right)}{k_{Aa} + k_{Ph} + k_S} \tag{35}$$

In Step 4 (M_s<T<T_g), the system is cooled below T_g but remains above M_s. The SMA is still contracted in its austenitic state, but the SMP has converted to its glassy state, helping to fix the position. The force in the SMP is calculated relative to its new neutral position x_{Pn2}, which is defined as the previous position multiplied by the shape fixity RF_P of the SMP. The position x_4 is calculated from the force balance (Figure 22a).

$$F_{A4} = k_{Aa}\left(x_4 - x_{An}\right), \quad F_{P4} = k_{Pl}\left(x_{Pn2} - x_4\right)$$
$$F_{S4} = k_S\left(L_S - L_0 - x_4\right), \quad x_{Pn2} = x_3 RF_P$$
$$x_4 = \frac{k_{Aa}x_{An} + k_{Pl}x_{Pn2} + k_S\left(L_S - L_0\right)}{k_{Aa} + k_{Pl} + k_S} \tag{36}$$

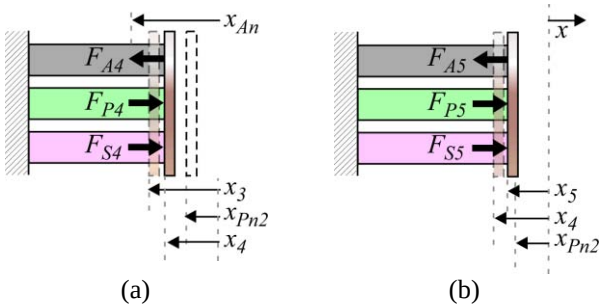

Figure 22. Two-way actuation: (a) step 4 and (b) step 5.

In Step 5 (T=RT<M_f), the system is cooled to room temperature while the SMA transforms from austenite to martensite. The SMP remains in its glassy state to hold the compressed position. The SMP has the same neutral position as in the previous step and the position x_5 can be calculated from the force balance (Figure 22b). This step results in the second room temperature fixed position*: martensite fixed compressed*.

$$F_{A5} = k_{Am}\left(L_0 - L_A + x_5\right), \quad F_{P5} = k_{Pl}\left(x_{Pn2} - x_5\right)$$
$$F_{S5} = k_S\left(L_S - L_0 - x_5\right)$$
$$x_5 = \frac{k_{Am}\left(L_A - L_0\right) + k_{Pl}x_{Pn2} + k_S\left(L_S - L_0\right)}{k_{Am} + k_{Pl} + k_S} \tag{37}$$

In Step 6 (T_g<T<A_s), the system is heated to above T_g but remains below A_s. The SMP converts to its rubbery state and allows the martensitic SMA to be stretched to its extended position. The system has returned to the same state as Step 0, with the position x_6≈x_0 found from the force balance (Figure 23).

$$F_{A6} = k_{Am}\left(L_0 - L_A + x_6\right), \quad F_{P6} = k_{Ph}\left(L_P - L_0 - x_6\right)$$
$$F_{S6} = k_S\left(L_S - L_0 - x_6\right)$$
$$x_6 = \frac{k_{Am}\left(L_A - L_0\right) + k_{Ph}\left(L_P - L_0\right) + k_S\left(L_S - L_0\right)}{k_{Am} + k_{Ph} + k_S} \tag{38}$$

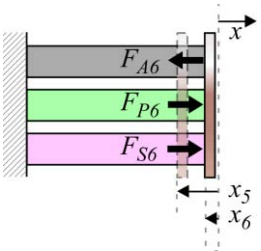

Figure 23. Two-way actuation: step 6.

Linear SMP-SMA Experimental Design

A linear end-coupled SMP-SMA experimental test setup has been designed to validate the linear shape fixity and two-way actuation models. Epoxy SMPs provide higher elastic moduli in their glassy state than polyurethane SMPs and have broader T_g range than styrene-based SMPs [14]. In addition, epoxy-based materials are easily manufactured and exhibit superior thermal and mechanical properties [15]. Xie and Rousseau [16] described an epoxy-based SMP with a tunable T_g. They showed that T_g can be decreased by increasing mol number of NGDE (Neopentyl glycol diglycidyl ether) and showed the shape fixity and shape recovery of epoxy samples with different mol ratios. The experimental setup that has been designed uses multiple Flexinol wires and a hollow cylindrically-shaped epoxy SMP. The SMP will be synthesized with the desired glass transition temperature relative to the SMA phase transitions to provide two-way actuation (2nd regime of SMC operation).

CONCLUDING REMARKS

Three regimes of SMC operation have been identified that capitalize on the characteristic shape fixity of SMPs and the shape recovery of SMAs. Initial SMC analyses showed that an SMP can hold an SMA spring with minimal deflection and quantified axial stresses in an SMA wire and SMP-SMA interfacial shear stresses. Simple analytical expressions for shape fixity were derived for a multi-layer SMC beam and end-coupled linear SMC system in extension.

COMSOL simulations show good agreement with the analytical expressions for shape fixity and interfacial shear stress of a multi-layer SMC beam. A model has been developed for the 2-way actuation regime of operation. A linear experimental setup has been designed and is being constructed to demonstrate 2-way actuation and validate the linear model.

REFERENCES

[1] Dietsch, B., and Tong, T., 2007, "A review-: Features and benefits of shape memory polymers (SMPs)," *Journal of Advanced Materials*, **39**(2), pp. 3–12.

[2] Gall, K., Mikulas, M., Munshi, N. A., Beavers, F., and Tupper, M., 2000, "Carbon fiber reinforced shape memory polymer composites," *Journal of Intelligent Material Systems and Structures*, **11**(11), pp. 877–886.

[3] Keihl, M. M., Bortolin, R. S., Sanders, B., Joshi, S., and Tidwell, Z., 2005, "Mechanical properties of shape memory polymers for morphing aircraft applications," *in Proceedings of SPIE*, **5762**, p. 143-151.

[4] Tobushi, H., Pieczyska, E., Ejiri, Y., and Sakuragi, T., 2009, "Thermomechanical Properties of Shape-Memory Alloy and Polymer and Their Composites," *Mechanics of Advanced Materials and Structures*, **16**(3), pp. 236–247.

[5] Tobushi, H., Hayashi, S., Hoshio, K., Makino, Y., and Miwa, N., 2006, "Bending actuation characteristics of shape memory composite with SMA and SMP," *Journal of Intelligent Material Systems and Structures*, **17**(12), pp. 1075–1081.

[6] Tobushi, H., Hayashi, S., Sugimoto, Y., and Date, K., 2009, "Two-way bending properties of shape memory composite with SMA and SMP," *Materials*, **2**(3), pp. 1180–1192.

[7] Brinson, L. C., and Huang, M. S., 1996, "Simplifications and comparisons of shape memory alloy constitutive models," *Journal of Intelligent Material Systems and Structures*, **7**(1), pp. 108–114.

[8] Bollas, D., Pappas, P., Parthenios, J., and Galiotis, C. , 2007, "Stress generation by shape memory alloy wires embedded in polymer composites," *Acta Materialia*, **55**(16), pp. 5489–5499.

[9] Hull, D., and Clyne, T. W., 1996, An introduction to composite materials, 2nd ed., New York: Cambridge University Press.

[10] Piggott, M., 2002, Load bearing fibre composites, 2nd ed., New York: Kluwer Academic Publishers.

[11] Hibbeler, R. C., 1997, Mechanics of materials, 3rd ed., New Jersey: Prentice Hall.

[12] TiNi Alloy Company, 2003, Introduction to Shape Memory Alloys, Retrieved March 10, 2012, from http://www. tinialloy.com/pdf/introductiontosma.pdf

[13] Khan, F., Koo, J. H., Monk, D., and Eisbrenner, E., 2008, "Characterization of shear deformation and strain recovery behavior in shape memory polymers," *Polymer Testing*, **27**(4), pp. 498–503.

[14] Leng, J., Lan, X., Liu, Y., and Du, S., 2011, "Shape-memory polymers and their composites: Stimulus methods and applications," *Progress in Materials Science*, **56**, pp. 1077-1135.

[15] Rousseau, I. A., and Xie, T., 2010, "Shape memory epoxy: Composition, structure, properties and shape memory performances," *Journal of Materials Chemistry*, **20**(17), pp. 3431–3441.

[16] Xie, T., and Rousseau, I. A., 2009, "Facile tailoring of thermal transition temperatures of epoxy shape memory polymers," *Polymer*, **50**(8), pp. 1852–1856.